



Available online at [www.sciencedirect.com](http://www.sciencedirect.com)

**jmr&t**  
Journal of Materials Research and Technology  
[www.jmrt.com.br](http://www.jmrt.com.br)



## Original Article

# Nanoscale structural investigation on Ti-6Al-4V implants produced by using selective laser melting technique: The importance of production angle

Ahmet Bayirli<sup>a</sup>, Semra Ide<sup>a,b,\*</sup>, Ilghar Orujalipour<sup>a</sup>, Osman Demir<sup>c</sup>, Murat Dursun<sup>c</sup>, Hakan Ates<sup>d</sup>

<sup>a</sup> Hacettepe University, Department of Nanotechnology and Nanomedicine, Beytepe, Ankara 06800, Turkey

<sup>b</sup> Hacettepe University, Department of Physics Engineering, Beytepe, Ankara 06800, Turkey

<sup>c</sup> Medical Design and Manufacturing Center, Gulhane Military Medical Academy, Etlik, Ankara 06010, Turkey

<sup>d</sup> Gazi University, Department of Metallurgical and Materials Engineering, Teknikokullar, Ankara 06500, Turkey

## ARTICLE INFO

### Article history:

Received 4 October 2018

Accepted 10 April 2019

Available online 17 May 2019

### Keywords:

Ti-6Al-4V

Small angle X-ray scattering

Selective Laser Melting

Build orientation

## ABSTRACT

Selective Laser Melting (SLM) is a powerful technique that enables us to produce complex shapes of implants customized for patients. Besides, all of the physicochemical effects on the structure of metal alloy implants must be taken under the control during the production such as polydispersity of the nanostructured morphologies inside of the incident metal alloy powders, orientation of the samples according to the growth axis, production temperature, the cooling methods of the produced implants, etc. In the present study, first case Small Angle X-Ray Scattering (SAXS) method was used on Ti-6Al-4V implants (produced by SLM technique) to nanostructurally investigate the orientation effect. Structural controls and characterizations leads more successful implant production related with nanoscale nucleations, grain aggregations and uniform distributions. So, the biophysical and biochemical properties of high corrosion resistive Ti-6Al-4V alloy implants would be able to be developed.

Initially the samples were examined by using SAXS, SEM-EDX techniques. An inside vision was tried to be gathered by calculating pair distance distribution functions (PDDF) and electron density distributions (EDD).

Analyzes showed that the orientation angles, except for 0° and 90°, lead to rough surface production, there were no impurities in the structures sourced by previously used nanopowders like cobalt or chrome beside of Ti-6Al-4V in the production system and the angles other than 0° and 90° increase the particle size but cause more homogenous structures. The best production angle was determined as 50° which lead to more uniform distributions and the more stable structures in nano and micro scales.

© 2019 The Authors. Published by Elsevier B.V. This is an open access article under the CC BY-NC-ND license (<http://creativecommons.org/licenses/by-nc-nd/4.0/>).

\* Corresponding author.

E-mail: [side@hacettepe.edu.tr](mailto:side@hacettepe.edu.tr) (S. Ide).

<https://doi.org/10.1016/j.jmrt.2019.04.019>

2238-7854/© 2019 The Authors. Published by Elsevier B.V. This is an open access article under the CC BY-NC-ND license (<http://creativecommons.org/licenses/by-nc-nd/4.0/>).

## 1. Introduction

Ti-6Al-4V (ASTM F136) alloy is widely preferred in implant sector because of the properties like biocompatibility, strength and lightweight<sup>1,2</sup> beside of its high corrosion resistance.<sup>3</sup>

Selective Laser Melting (SLM) is a powerful technique to produce Ti-6Al-4V alloy implants and this technique enables us to produce complex shaped implants for special and characteristic patients.<sup>4</sup> Fundamental knowledge may be briefly given in this phase, to understand the importance of nano scale structural controls and characterizations. The 3D printing technique uses nanostructured raw metal alloy powders as incident materials and a laser source fundamentally used to melt these powders layer by layer approach. Implant productions are designed with a CAD software and mapped into layers. These maps are fed into SLM machine.<sup>5</sup> There are various parameters effecting the structure of final product like wavelength of laser,<sup>6</sup> powder layer thickness,<sup>7</sup> scanning pattern,<sup>8</sup> scanning speed,<sup>9</sup> scan line spacing,<sup>10</sup> build orientation,<sup>11</sup> post-process annealing temperature,<sup>12</sup> cooling technique,<sup>13</sup> etc.<sup>14</sup> These parameters are tried to be optimized to increase the properties of products such as strength, biocompatibility, etc.<sup>15</sup> So it can be said that, the nanoscale nucleations and starting points of the nano and micro sized

scattering vector magnitude of  $q$  ( $q = (4\pi/\lambda) \sin\theta$ ;  $\theta$  is the scattering angle). Scattered data may be collected in the scattering angle range of  $0.1^\circ$ – $20^\circ$  and the data is related with the reciprocal space. PDDF can be calculated by inverse Fourier transform of the scattering data to reach real space information. PDDF gives information about maximum particle size, radius of gyration and particle shape.<sup>21–23</sup> EDD can be also calculated for the other detailed SAXS analyses in electron density level from PDDF via convolution square root method.<sup>24</sup> EDD is the average distribution in one radial direction and mostly gives the structural details including intra-particle information.

Since PDDF and EDD were calculated for the poly dispersed hard sphere model as the best convenient form factors of the nano aggregations in the implant structures.

The structural model of poly-dispersed hard sphere may be defined by Eqs. (1) and (2).<sup>25</sup>

$$I(Q) = \eta V(\Delta\rho)^2 \int_0^\infty F_i^2(Q, \sigma_i) f(\sigma_i) d\sigma_i \quad (1)$$

$$F_i(Q, \sigma_i) = 4\pi [\sin(Q\sigma_i/2) - (1/2)Q\sigma_i \cos(Q\sigma_i/2)] \quad (2)$$

$I(Q)$  equation is used to model the implant clusters, assuming that the polydispersed spheres have Schultz size

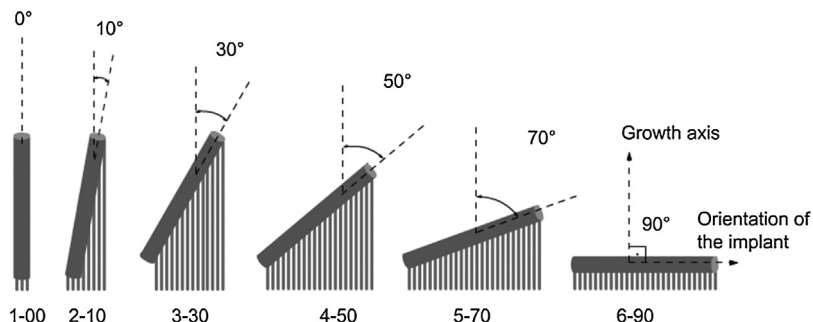


Fig. 1 – Illustration of the production angles and the sample codes.

grains play important roles in structure-properties correlations of the produced implants.

During SLM process, SLM machine lays powder in determined thickness and melts determined points for each layer of products. Since the SLM machine does not know the orientation of products, we may choose any angle we desire as long as final product fits into the limitations of the machine. As orientation of product changes, orientation of layers remains same. This leads different step sizes on surface of same products with different orientations. This is called stair-step-effect<sup>16</sup> and there are various articles examining this effect on the surface<sup>17</sup> and the mechanical properties of products like fatigue resistance,<sup>18</sup> crack propagation,<sup>19</sup> etc. In the present study, we investigated the nano structural characteristics of the focused implant materials and the effect of the implant orientation respect to the growth axis in the production system. The used Small Angle X-ray Scattering (SAXS) technique has big advantages to investigate the nanostructured materials.<sup>20</sup> In this method, monochromatic X-rays are sent through sample as incident beam and the intensities,  $I(q)$ , of the elastic scattered X-rays are collected as a function of the

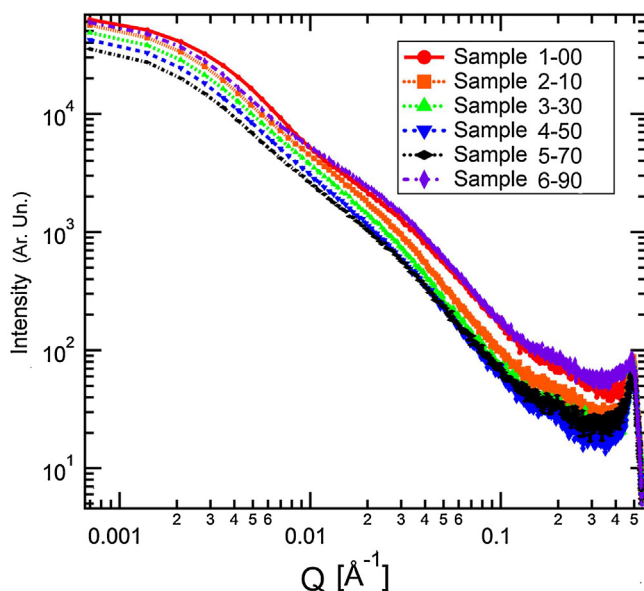


Fig. 2 – SAXS profiles of the studied samples.

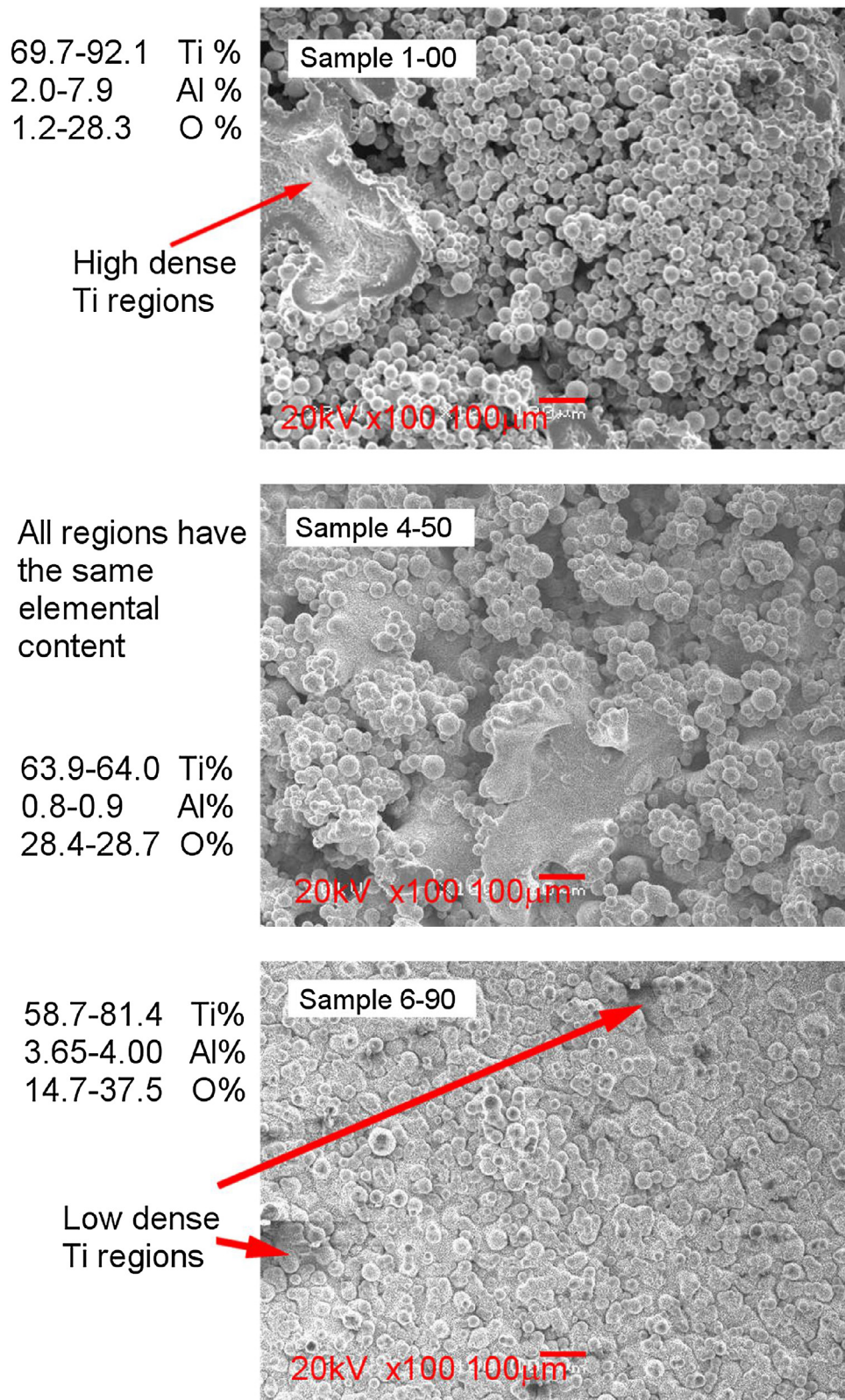
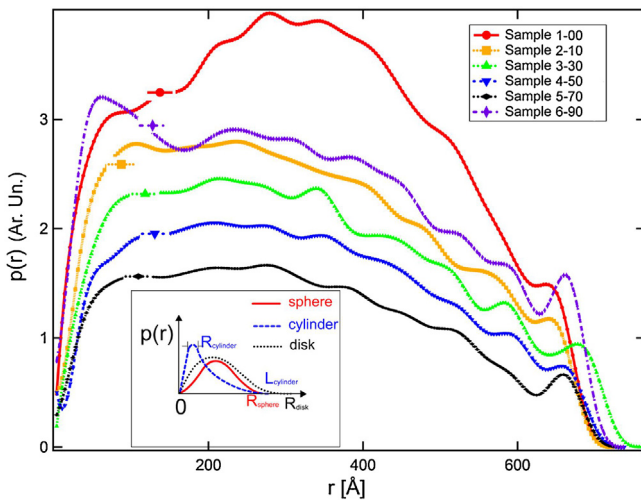


Fig. 3 – SEM images and EDX results for Sample 1-00, Sample 4-50 and Sample 6-90 (indicating small, medium, and large production angles).



**Fig. 4 –** The calculated PDDFs ( $p(r)$ ) as a function of the radial distance of  $r$ : an ideal monodispersed nanostructured sample shows a smooth hump.

distribution with hard-sphere interaction between clusters,  $\eta$  is the volume fraction of the clusters, and  $\Delta\rho$  is the difference in scattering length density (SLD) between the clusters and surrounding matrix.  $V$  is the average cluster volume.  $F(Q, \sigma_i)^2$  is the form factor of the spherical cluster with a diameter  $\sigma_i$ .  $R$  is the mean cluster radius included by the diameter. The polydispersity,  $p$ , is defined as  $a/R$ , where  $a^2$  is the variance of the Schultz size distribution  $f(\sigma)$ .

Above mentioned  $I(Q)$  equation and the model were well fitted to the scattering data.

## 2. Samples

Ti-6Al-4V alloy implants were produced in Gulhane Military Medical Academy, Center of Medical Design and Manufacturing (GATA-METUM) using Concept Laser M2 Cusing Machine. Samples were annealed at 840 °C for 5 h and then cooled down in furnace. 6 different cylindrical samples (with diameter of 2 mm and length of 15 mm) were produced with different orientation angles, 0°, 10°, 30°, 50°, 70°, 90° respectively as seen in Fig. 1. Needle like place holders of the samples were removed and cleaned from the surface of the cylinders before the SAXS analyses.

SLM (Selective Laser Melting) steps were followed as explained here,

1. CAD (Computer Aided Design) data of the target piece is prepared and transformed to STL (StereoLitography) data.
2. STL data is virtually sliced into 30 µm layers and also supportive bars are placed between 3D design and production table. Final design is fed to the SLM machine with a file of \*.cls extension.
3. SLM machine lays out a 30 µm thick layer of Ti-6Al-4V powder onto production table and melts the designed points on the layer with a CO<sub>2</sub>/fiber laser. Every layer defined in the \*.cls file is interpreted one by one and processed by repeating the step 3.

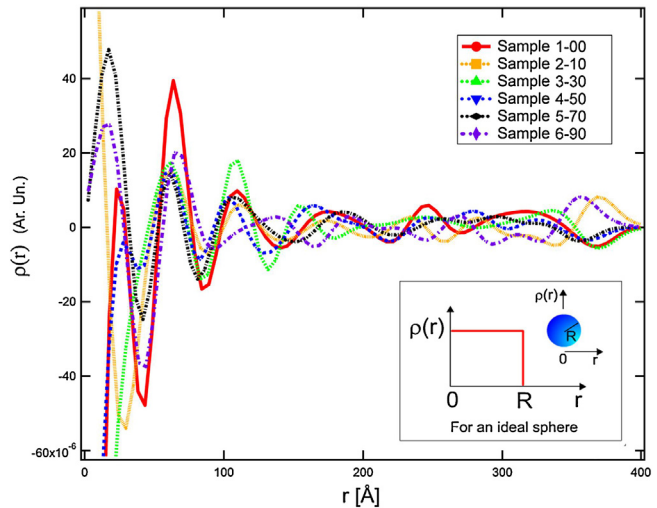


**Fig. 5 –** Electron density distributions calculated from PDDFs of samples and a view of the ideal case: the fluctuations are not wanted for the uniform implants.

4. At the end of the process, remaining powders are collected and returned to the initial tank. Production table is removed. Products may need further cleaning from powders. And also supportive bars are removed too.
5. In order to release the stress, products were annealed and cooled down. Samples were annealed at 840 °C for 5 h in an argon filled oven. They were left to cool down in oven.

## 3. Methods

SEM images of samples were initially taken in order to monitor changes on the surface. JEOL JSM-6060 LW SEM device were used and also EDX analysis were carried out to search impurities while SWAXS methods were used in order to investigate nano-structure.

SAXS profiles were measured by a Kratky compact Hecus system with 1024 channel detectors and line collimation of CuK<sub>α</sub> ( $\lambda = 1.54 \text{ \AA}$ ). Distances between channels and the sample to detector are 54 µm and 31.5 cm, respectively. All samples were measured for 4 times 300 s at 23 °C by using a convenient sample holder of the system in transmission mode. Four measurement results for each sample averaged to reduce the noise.

SAXS data (Fig. 2) were evaluated by using various software such as IGOR Pro, PCG-GIFT and PCG-Decon to fit the model and calculate the pair distance and electron density distributions.

A preliminary examination can be done directly comparing the SAXS results of the samples. It can be seen in Fig. 2 that there is a hump on  $0.01\text{--}0.1 \text{ \AA}^{-1}$  region which means that there are nano-sized aggregations in the sample and also the difference between intensities of humps for different samples can be interpreted as production angle affects the nano structure.

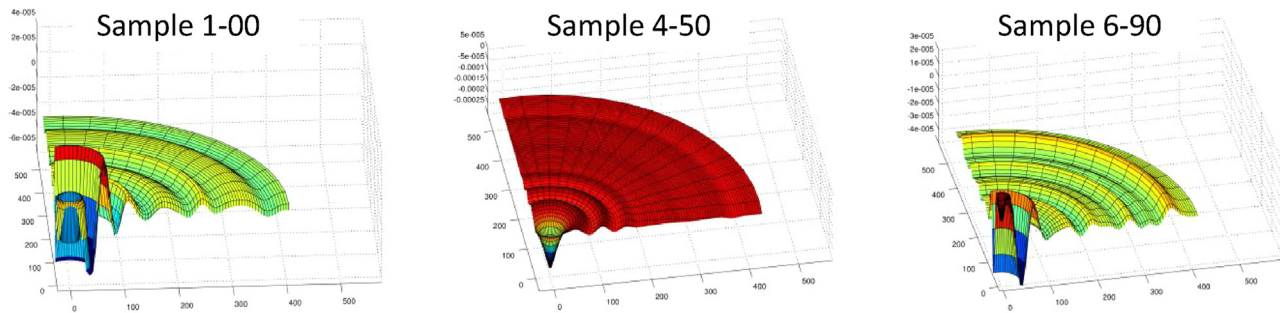


**Fig. 6 – 3D electron density distributions of the samples which have the production angles of 0, 50 and 90°.**

#### 4. Results

SEM images and EDX results are shown in Fig. 3. It can be observed in SEM images too that the production angle affects the structure.

PDDF and EDD of the samples were calculated by using SAXS data and the distributions were given as seen in Figs. 4 and 5, respectively.

According to Fig. 4, it may be said that, Sample 4-50 has better (low polydispersed and more uniform) structure. Since we are looking for the resemblance and convenience to PDD of the perfect sphere formation. The shape of the hump is smoother than the other PDDs and the obtained radii value of the nanoglobules which are main structural unit of this sample has smaller accuracy.

The calculated PDDFs of the nanoglobules (polydisperse hard spheres) aggregates in the structures may be seen in Fig. 5. EDD results were also calculated by using PCG-DECON as shown in Fig. 6.

The more uniform structure may be also easily seen in that of Sample 4-50.

#### 5. Conclusions

Ti-6Al-4V implants produced via Selective Laser Melting were studied. Effects of build orientation observed in micro and nano scale structural analyses.

The effects of the build orientation on the surface of the samples can be seen from the SEM images. The effects on the nano structures can be obtained and compared with PDDFs and EDDs.

As a general result, it can be said that the best sample is produced with the production angle of 50°. At the same time, Sample 4-50 has more compact structure and more uniform electron density distribution. According to the all studied angles, we may say that homogeneity is increased with production until 50° and then it is decreased.

SEM results showed that surface directly affected by build orientation. The prepared implant samples were in cylindrical forms as outer shape and larger surface facing to the laser was during 90°. We may say that the bigger production angle causes the smoother surface.

#### Conflicts of interest

The authors declare no conflicts of interest.

#### REFERENCES

- [1] Niinomi M. Mechanical biocompatibilities of titanium alloys for biomedical applications. *J Mech Behav Biomed Mater* 2008;1:30–42, <http://dx.doi.org/10.1016/j.jmbbm.2007.07.001>.
- [2] Geetha M, Singh aK, Asokamani R, Gogia aK. Ti based biomaterials, the ultimate choice for orthopaedic implants – A review. *Prog Mater Sci* 2009;54:397–425, <http://dx.doi.org/10.1016/j.pmatsci.2008.06.004>.
- [3] Zhao B, Wang H, Qiao N, Wang C, Hu M. Corrosion resistance characteristics of a Ti-6Al-4V alloy scaffold that is fabricated by electron beam melting and selective laser melting for implantation in vivo. *Mater Sci Eng C* 2017, <http://dx.doi.org/10.1016/j.msec.2016.07.045>.
- [4] Krauss H, Zaeh M. Investigations on manufacturability and process reliability of selective laser melting. *Phys Procedia* 2013;41:808–15.
- [5] Kumar S. Comprehensive Materials Processing, vol. 10. Elsevier; 2014, <http://dx.doi.org/10.1016/B978-0-08-096532-1.01003-7>.
- [6] Yadroitsev I, Smurov I. Selective laser melting technology: from the single laser melted track stability to 3D parts of complex shape. *Phys Procedia* 2010;5:551–60, <http://dx.doi.org/10.1016/j.phpro.2010.08.083>.
- [7] Yadroitsev I, Bertrand P, Smurov I. Parametric analysis of the selective laser melting process. *Appl Surf Sci* 2007;253:8064–9, <http://dx.doi.org/10.1016/j.apsusc.2007.02.088>.
- [8] Thijss L, Verhaeghe F, Craeghs T, Van Humbeeck J, Kruth J-P. A study of the microstructural evolution during selective laser melting of Ti-6Al-4V. *Acta Mater* 2010;58:3303–12, <http://dx.doi.org/10.1016/j.actamat.2010.02.004>.
- [9] Song B, Dong S, Zhang B, Liao H, Coddet C. Effects of processing parameters on microstructure and mechanical property of selective laser melted Ti6Al4V. *Mater Des* 2012;35:120–5, <http://dx.doi.org/10.1016/j.matdes.2011.09.051>.
- [10] Zhang S, Wei Q, Cheng L, Li S, Shi Y. Effects of scan line spacing on pore characteristics and mechanical properties of porous Ti6Al4V implants fabricated by selective laser melting. *Mater Des* 2014;63:185–93, <http://dx.doi.org/10.1016/j.matdes.2014.05.021>.
- [11] Simonelli M, Tse YY, Tuck C. Effect of the build orientation on the mechanical properties and fracture modes of SLM

- Ti-6Al-4V. *Mater Sci Eng A* 2014;616:1–11, <http://dx.doi.org/10.1016/j.msea.2014.07.086>.
- [12] Wauthle R, Vrancken B, Beynaerts B, Jorissen K, Schrooten J, Kruth J-P, et al. Effects of build orientation and heat treatment on the microstructure and mechanical properties of selective laser melted Ti6Al4V lattice structures. *Addit Manuf* 2014;5:77–84, <http://dx.doi.org/10.1016/j.addma.2014.12.008>.
- [13] Vrancken B, Thijs L, Kruth J-P, Van Humbeeck J. Heat treatment of Ti6Al4V produced by Selective Laser Melting: microstructure and mechanical properties. *J Alloys Compd* 2012;541:177–85, <http://dx.doi.org/10.1016/j.jallcom.2012.07.022>.
- [14] Hanzl P, Zetek M, Bakša T, Kroupa T. The Influence of Processing Parameters on the Mechanical Properties of SLM Parts. *Procedia Eng* 2015;100:1405–13, <http://dx.doi.org/10.1016/j.proeng.2015.01.510>.
- [15] Sun J, Yang Y, Wang D. Parametric optimization of selective laser melting for forming Ti6Al4V samples by Taguchi method. *Opt Laser Technol* 2013;49:118–24.
- [16] Kruth J, Vandenbroucke B, Vaerenbergh J, Naert I. Rapid manufacturing of dental prostheses by means of selective laser sintering/melting. *Int Conf Adv Res Virtual Rapid Prototyp 2005*.
- [17] Yadroitsev I, Smurov I. Surface morphology in selective laser melting of metal powders. *Phys Procedia* 2011;12:264–70, <http://dx.doi.org/10.1016/j.phpro.2011.03.034>.
- [18] Leuders S, Thöne M, Riemer a, Niendorf T, Tröster T, Richard HA, et al. On the mechanical behaviour of titanium alloy TiAl6V4 manufactured by selective laser melting: fatigue resistance and crack growth performance. *Int J Fatigue* 2013;48:300–7, <http://dx.doi.org/10.1016/j.ijfatigue.2012.11.011>.
- [19] Cain V, Thijs L, Van Humbeeck J, Van Hooreweder B, Knutsen R. Crack propagation and fracture toughness of Ti6Al4V alloy produced by selective laser melting. *Addit Manuf* 2014;5:68–76, <http://dx.doi.org/10.1016/j.addma.2014.12.006>.
- [20] Portale G, Longo A. Small-Angle X-ray Scattering for the Study of Nanostructures and Nanostructured Materials; 2013.
- [21] Glatter O. The Interpretation of Real-Space Information from Small-Angle Scattering Experiments. *J Appl Cryst* 1979;12:166–75.
- [22] Bergmann A, Fritz G, Glatter O. Solving the generalized indirect Fourier transformation (GIFT) by Boltzmann simplex simulated annealing (BSSA). *J Appl Crystallogr* 2000;33:1212–6, <http://dx.doi.org/10.1107/S0021889800008372>.
- [23] Glatter O, Brunner-Popela J. *J. Appl. Cryst* 1997;30:431–42. Small-Angle Scattering of Interacting Particles. I. Basic Principles of a Global Evaluation Technique. *J Appl Cryst* 1997;30:431–42.
- [24] Glatter O. Convolution Square Root of Band-Limited Symmetrical Functions and its Application to Small-Angle Scattering Data. *J Appl Cryst* 1981;10:1–8.
- [25] Liao H-C, Tsao C-S, Lin T-H, Chuang C-M, Chen C-Y, Jeng U-S, et al. Quantitative Nanoorganized Structural Evolution for a High Efficiency Bulk Heterojunction Polymer Solar Cell. *J Am Chem Soc* 2011, <http://dx.doi.org/10.1021/ja202977r>.